HHS Public Access

Author manuscript

J Med Chem. Author manuscript; available in PMC 2020 February 28.

Published in final edited form as:

J Med Chem. 2019 February 28; 62(4): 2008–2023. doi:10.1021/acs.jmedchem.8b01573.

Structural basis of altered potency and efficacy displayed by a major *in vivo* metabolite of the anti-diabetic PPARγ drug pioglitazone

Sarah A. Mosure[1,2], **Jinsai Shang**[2], **Jerome Eberhardt**[3], **Richard Brust**[2], **Jie Zheng**[4], **Patrick R. Griffin**[2,4], **Stefano Forli**[3], **Douglas J. Kojetin**[2,4,*]

[1]Skaggs Graduate School of Chemical and Biological Sciences, The Scripps Research Institute, Jupiter, Florida 33458, USA

[2]Department of Integrative Structural and Computational Biology, The Scripps Research Institute, Jupiter, Florida 33458, USA

[3]Department of Integrative Structural and Computational Biology, The Scripps Research Institute, La Jolla, California 92037, USA

[4]Department of Molecular Medicine, The Scripps Research, Jupiter, Florida 33458, USA

Abstract

Pioglitazone (Pio) is an FDA-approved drug for type 2 diabetes that binds and activates the nuclear receptor PPARγ. yet it remains unclear how *in vivo* Pio metabolites affect PPARγ structure and function. Here, we present a structure-function comparison of Pio and its most abundant *in vivo* metabolite, 1-hydroxypioglitazone (PioOH). PioOH displayed a lower binding affinity and reduced potency in coregulator recruitment assays. X-ray crystallography and molecular docking analysis of PioOH-bound PPARγ ligand-binding domain (LBD) revealed an altered hydrogen bonding network, including formation of water-mediated bonds that could underlie its altered biochemical phenotype. NMR spectroscopy and hydrogen/deuterium exchange mass spectrometry (HDX-MS) analysis coupled to activity assays revealed that PioOH better stabilizes the PPARγ activation function-2 (AF-2) coactivator binding surface and better enhances coactivator binding, affording slightly better transcriptional efficacy. These results indicating Pio hydroxylation affects its potency and efficacy as a PPARγ agonist contribute to our understanding of PPARγ-drug metabolite interactions.

Graphical Abstract

[*]**Corresponding Author Information:** dkojetin@scripps.edu; Tel. (561) 228-2298; Fax. (561) 228-2297.

Associated Content

Supporting Information

Molecular formula strings in csv file. Differential HDX-MS data for peptides analyzed.

PDB ID Codes

Structure factors and atomic coordinates have been deposited in the Protein Data Bank under accession code 6DHA. Authors will release the atomic coordinates and experimental data upon article publication

The authors declare that they have no conflicts of interest with the contents of this article.

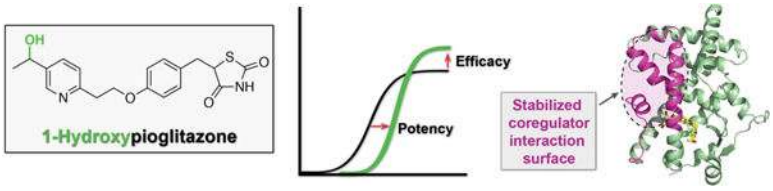

Keywords

ligand-binding protein; drug metabolism; X-ray crystallography; nuclear magnetic resonance (NMR); hydrogen exchange mass spectrometry (HDX-MS); peroxisome proliferator-activated receptor gamma (PPARγ); ligand-binding domain (LBD); nuclear receptor; gene transcription

Introduction

The thiazolidinedione (TZD) pioglitazone (Pio) is an FDA-approved drug for the treatment of type 2 diabetes [1]. Pio binds and activates peroxisome proliferator-activated receptor gamma (PPARγ), a nuclear receptor transcription factor that regulates expression of genes important for insulin sensitivity, lipid metabolism, and inflammation [2]. PPARγ has the conserved nuclear receptor domain architecture comprised of an N-terminal activation function-1 (AF-1) domain, a DNA-binding domain (DBD), a flexible hinge region, and C-terminal ligand-binding domain (LBD) [3]. The DBD recognizes and binds PPAR response elements (PPREs) within the promoter region of target genes, and although DNA binding has been shown to affect receptor function [4–7], the PPARγ LBD has been the primary focus for developing therapeutics because endogenous lipids and synthetic small molecule ligands such as TZDs bind to the LBD and regulate the transcriptional activity of PPARγ.

The PPARγ LBD contains 12 α-helical structural elements that form a three-layer sandwich fold; within this fold is a large hydrophobic core known as the canonical or orthosteric ligand binding pocket. Adjacent to the ligand-binding pocket, a surface formed by the three-dimensional association of helix 3 (h3), helix 4 (h4), helix 5 (h5), and helix 12 (h12) is called the activation function-2 (AF-2) coregulator interaction surface [8, 9]. Conformational changes in the AF-2 surface that occur in response to ligand binding mediate interactions with coregulators that influence recruitment of chromatin-modifying enzymes and other transcriptional machinery to control downstream gene expression. In the absence of an activating (agonist) ligand, PPARγ recruits transcriptionally repressive corepressor complexes including proteins such as Nuclear Receptor Corepressor 1 (NCoR1) [1, 10]. However, when an agonist binds to the PPARγ ligand-binding pocket, the AF-2 surface is stabilized, favoring loss of the corepressor complex and recruitment of coactivator proteins such as Thyroid hormone Receptor Associated Protein 220 (TRAP220) [11–13]. Previous studies sought to characterize the mechanisms by which agonists activate PPARγ, with early evidence suggesting that h12 acts as a simple “on/off” switch [14]. Recent investigations support more complex mechanisms by which ligands regulate PPARγ function: for instance, by affecting LBD conformational dynamics [11, 15, 16], binding to an alternate/allosteric site within the LBD [12, 17], or regulating post-translational modifications of PPARγ [18, 19].

Full PPARγ agonists like the TZDs stabilize an active AF-2 surface conformation through a hydrogen bond network with residues near helix 12 including S289, H323, H449, and Y473 [20]. Because Pio is known to have deleterious side effects such as weight gain and musculoskeletal complications, there is demand for a more sophisticated understanding of its effects on PPARγ structure and function [21]. One area that requires further investigation is the effects of *in vivo* Pio metabolites. Small molecules like Pio are chemically modified by liver cytochrome P450 enzymes to facilitate excretion [22, 23]. These modified metabolic intermediates can enter systemic circulation and often persist longer than the original drug [24]. Some TZD metabolites maintain the ability to bind and activate PPARγ [23], but enzymatic addition of functional groups may lead to differential regulation of PPARγ activity. Rezulin/troglitazone, another previously FDA-approved TZD for the treatment of T2DM, was removed from the market after a major metabolite caused hepatotoxicity [22]. Therefore, it is critical to characterize the metabolites of FDA-approved drugs like Pio as well as the original small molecule.

Previous pharmacokinetic analyses of Pio (Fig. 1A) identified several major *in vivo* PioOH metabolites (Fig. S1), including the most abundant metabolite 1-hydroxypioglitazone (PioOH) (Fig. 1A), which exhibited weaker anti-hyperglycemic effects despite differing from Pio only by the addition of a hydroxyl group [25, 26]. Human studies found that the PioOH half-life and total body exposure is about triple that of Pio [24]. These findings suggest that a significant portion of Pio's effects could be from PioOH, emphasizing this metabolite's physiological relevance. Yet, to our knowledge, it remains unknown how Pio hydroxylation directly affects its activity on PPARγ. Here, we investigated how the functional effects of PioOH are related to its structural interaction with the PPARγ LBD. Using biochemical and cellular transactivation assays, we showed that Pio hydroxylation reduces potency, as demonstrated by increased EC_{50}/IC_{50} values in transactivation and coregulator recruitment assays, which may explain its reduced anti-hyperglycemic effects relative to Pio *in vivo*. We solved the crystal structure of PioOH-bound PPARγ LBD, which we used to perform molecular docking comparison of Pio metabolites and their stereoisomers, which together identified changes in the ligand-receptor hydrogen bonding network that may underlie PioOH's reduced potency. Our solution-state structural analysis using protein NMR and HDX-MS revealed that PioOH stabilized the dynamics of the AF-2 surface compared to Pio. Stabilization of AF-2 surface dynamics was associated with changes in the thermodynamics of coactivator binding and enhanced efficacy in a chimeric cellular transcription assay that reports on the activity of the PPARγ LBD. Overall, these findings contribute to our understanding of how synthetic ligands and their *in vivo* metabolites fine-tune PPARγ function.

Results

PioOH has a weaker binding affinity and coregulator recruitment potency than Pio

We first assessed the binding affinity of Pio and PioOH (Fig. 1A) to the PPARγ LBD using a fluorescent ligand displacement assay (Fig. 1B), which revealed that the metabolic conversion of Pio to PioOH via addition of a hydroxyl group to the end of the hydrophobic side chain of Pio weakened the interaction with the PPARγ LBD. CD spectroscopy thermal

denaturation experiments confirmed binding and revealed that the unfolding temperature of the PPARγ LBD is increased upon binding both Pio and PioOH (Fig. 1C), indicating binding of these ligands stabilized the LBD. We also performed time resolved fluorescence resonance energy transfer (TR-FRET) biochemical assays to determine how Pio and PioOH affect the interaction with peptides derived from a PPARγ-interacting transcriptional coactivator (TRAP220) and corepressor (NCoR1). Consistent with its reduced binding affinity, PioOH was less potent than Pio in recruiting the TRAP220 peptide (Fig. 1D) and displacing the NCoR1 peptide (Fig. 1E).

Crystal structure of PioOH-bound PPARγ LBD reveals an altered hydrogen bonding network

To determine the structural basis of PioOH activity compared to Pio, we solved the crystal structure of PPARγ LBD bound to PioOH at 1.88 Å resolution using molecular replacement (Table 1). The X-ray crystal structure of Pio bound to PPARγ LBD was recently solved at comparable resolution (1.80 Å; PDB code 5Y2O) [20]. Both Pio and PioOH-bound PPARγ LBDs crystallized as dimers: h12 in chain A adopts an "active" conformation with the ligand bound in the orthosteric pocket, whereas h12 in chain B adopts an atypical conformation in which h12 docks onto adjacent molecules within the crystal lattice. Structural alignment of Pio- vs. PioOH-bound chain A resulted in an overall rmsd of 0.39 Å (Fig. 2A), indicating there were no overt structural changes. However, we observed subtle structural changes that could explain the reduced affinity of PioOH.

The TZD head group of both ligands form hydrogen bonds and weak electrostatic interactions with the side chains of residues Q286, S289, H323, H449, and Y473. The PioOH TZD head group was tilted ~0.9 Å such that the interacting side chains S289, H449, and Y473 were farther from their hydrogen bond donor/acceptor, while Q286 and H323 were closer in the PioOH-bound structure despite overall minimal changes in side chain conformations (Fig. 2B–D). The PioOH TZD head group displacement was reciprocated by a 0.9 Å shift of h12 away from h3 and a 1.1 Å shift of h11 toward h3 (Fig. 2A,B). The PioOH hydroxyl group formed a weak water-mediated hydrogen bond via HOH709 with the side chain of S342 (Fig. 2C), which may have contributed to the shifted TZD head group of PioOH relative to Pio. The water-mediated hydrogen bond is also likely responsible for the shifted binding pose of the terminal methyl group towards G284 on helix 3 (Fig. 2C,D). However, this methyl shift did not introduce any steric clashes with residues near helix 3 that might weaken the affinity. We also observed a water-bridged hydrogen bond (via HOH628 and HOH692) between the PioOH pyridinyl nitrogen and the S342 backbone nitrogen (Fig. 2C). In contrast, the pyridinyl nitrogen in the Pio structure was previously modeled inward toward the ligand binding pocket and examination of the density did not show the presence of any bridging water molecules (Fig. 2D). Thus, the weak water-mediated hydrogen bonds introduced by Pio hydroxylation may drive the TZD head group shift and contribute to the weakened affinity and potency of PioOH.

Molecular docking reveals conserved binding mode of Pio metabolites and stereoisomers

Although Pio and PioOH exist as racemic mixtures both in our experiments and *in vivo* [24], the crystallized binding modes favored a single stereoisomer: (*S*)-TZD and (1*S*)-PioOH.

Molecular docking studies of other synthetic PPARγ ligands have successfully predicted the binding poses of compounds with varied moieties [27, 28]. Thus, to investigate alternative enantiomer binding modes, we performed molecular docking analyses for the enantiomers/stereoisomers of Pio, PioOH, and those of the other previously reported Pio metabolites: M-I, M-II, M-III, M-V, and M-VI (Fig. S1) [26]. Results were visually inspected and compared to the crystallographic coordinates of (*S*, *S*)-PioOH, assuming all the metabolites bind in a similar manner. The docking results showed that metabolites with the (*S*)-TZD ring established more favorable interactions in the receptor pocket, presenting ~5-fold lower binding energies than the (*R*)-isomers within the error of the docking scoring function (Tables 2–5). The (*R*)-TZD isomer was unable to form the conserved hydrogen bonds with residues H323 and S286, and interactions with Y473 and H449 were weakened (Fig. 3A vs. Fig. 2C). These results are in agreement with a previously reported rosiglitazone competition binding assay that showed higher affinity for (*S*)-Rosiglitazone than (*R*)-Rosiglitazone [29], indicating that TZD head group stereochemistry affects binding to PPARγ LBD.

Pio hydroxylation creates a second chiral center in metabolites M-II and M-IV (PioOH). Unlike the effect of the chirality of the TZD head group, the chirality of the tail was not a significant factor in the binding scores. For example, no significant differences were found in the predicted binding modes of (*S*, *S*)-PioOH and (*S*, *R*)-PioOH. While the enantiomer (*S*, *S*)-PioOH interacts with S342 through the bridging water molecule HOH709, the enantiomer (*S*, *R*)-PioOH might maintain its binding affinity by directly interacting with the backbone carbonyl oxygen of I281 located on helix 3 (Fig. 3A).

We also investigated the roles of bridging waters HOH709, HOH628, and HOH692 identified in the PioOH-bound crystal structure. Though they did not affect the binding mode of the TZD head group (Tables 2–5), the water molecules affected the placement of the chains extending toward the β-sheet. In the absence of the bridging waters, the crystal pose of (*S*, *S*)-PioOH could not be reproduced (Table 2 and Fig. 3B). HOH709 had a greater influence than HOH628 and HOH692 on reproducing the crystallographic pose, particularly the tail of (*S*, *S*)-PioOH (Tables 2,3 and Fig. 3C,D). Analysis of 13 other previously reported ligand-bound PPARγ LBD crystal structures available in the PDB with a pyridinyl group close to the S342 backbone nitrogen indicated that the presence of the HOH628 and HOH692 water molecules is not conserved: only three of the structures (1FM6 chain D, 2PRG chain A, and 5YCP chain A) shared a similar interaction pattern as (*S*, *S*)-PioOH with the S342 backbone nitrogen. Four structures (1FM6 chain X, 2PRG chain B, 3CS8 chain A, and 4O8F chain B) did not show any bridging water molecules. Two structures (3DZY chain D and 4O8F chain A) showed a direct interaction with the R288 side chain. Two structures (4XLD chain A and 5JIO chain D) showed the presence of a water molecule but with the nitrogen atom pointing inward toward the ligand binding pocket, and two structures (5Y2O and 4EMA), which includes the Pio-bound structure, showed the nitrogen atom pointing inward and no bridging water. Together, these results may explain the minimal impact of HOH628 and HOH692 on the docking performance, and further indicate that the water-mediated hydrogen bond with the S342 side chain has the more critical role in PioOH binding.

The other Pio metabolites exhibited a similar pattern in their enantiomer binding modes. As might be expected, M-I binding affinity was unaffected by the presence of the water molecules during the docking procedure, as it lacks a tail extending toward the β-sheet. It also bound with ~100-fold lower affinity than the other metabolites (Tables 2–5), consistent with previous reports indicating M-I is not an active Pio metabolite [24]. Notably, the M-V and M-VI metabolites, which are also thought to be inactive due to a lack of anti-hyperglycemic activity when administered to mice [26], bound with affinities comparable to active metabolites PioOH, M-III, and M-II (Tables 3–5). The high predicted affinities may be an artifact of the docking procedure, or the molecules may bind with high affinity to PPARγ, but lack efficacy as PPARγ agonists or do not achieve sufficient cellular penetrance to produce transcriptional activation *in vivo.*

Solution structural analysis reveals enhanced AF-2 stabilization by PioOH

Although ligand-bound crystal structures provide important molecular detail into the binding mode of PPARγ ligands, it has been difficult to identify structural mechanisms of graded ligand activity, such as full vs. partial agonism, due to the structural homogeneity of protein conformations within the crystals [30]. Typically, backbone conformations observed in ligand-bound PPARγ crystal structures are highly similar due to crystal packing forces that favor the most stable crystallized conformation, and thus they are not representative of the ensemble of conformations present in solution. Alternatively, structural studies that probe the dynamics of proteins in solution, such as NMR spectroscopy and HDX-MS, have identified more nuanced yet functionally relevant characteristics of graded activation [11, 15, 16].

We performed differential NMR analysis by collecting 2D [^{1}H,^{15}N]-TROSY-HSQC NMR spectra of ^{15}N-labeled PPARγ LBD with Pio or PioOH (Fig. 4A). NMR peaks were assigned to residues using the minimal NMR chemical shift method [31] based on their nearest neighbor to rosiglitazone-bound PPARγ LBD NMR chemical shift assignments [11]. This method allowed us to assign 181 well-resolved peaks for PioOH and Pio; 93 residues remained unassigned mostly due to NMR peak overlap that made transfer of NMR assignments difficult (Fig. 4B). We calculated NMR chemical shift perturbations (CSPs) between the Pio- and PioOH-bound states to identify changes in the chemical environment of PPARγ LBD (Fig. 4C), which can be due to differences in residues that directly contact the ligands as well as allosteric conformational differences that occur between Pio- and Pio-OH bound PPARγ LBD. There were eight residues with CSPs more than two standard deviations (CSP > 0.037 p.p.m.) from the mean CSP (0.013 p.p.m.) (Fig. 4B,C). These residues were located primarily in the β-sheet region (L340, I341, G346, and V248) (Fig. 5A and B), or at the putative site of ligand entry/exit [32], a region comprised of the h6–7 loop (F360 and D362) and the N-terminus of h3 (A278 and I279) (Fig. 5C and D). Another residue with a significant CSP (I262) was located in the Ω-loop, a flexible region between h2 and h3 absent from most PPARγ LBD crystal structures.

The CSPs between Pio and PioOH-bound PPARγ observed for the β-sheet region were consistent with the water-mediated hydrogen bond observed in the PioOH-bound crystal structure between the PioOH hydroxyl group and the S342 side chain, which is not present

in the Pio-bound structure. Although the crystal structures only showed minor structural changes (~0.5 Å) in the backbone and negligible side chain alterations, the water-mediated hydrogen bond affected the chemical environment of residues in this region, as detected by NMR (Fig. 5A,B and 4B). At the same time, residues with CSPs near the h6–7 loop were reflected by structural changes in the crystal structures: there was a 0.8 Å shift of the h6–7 loop toward h3 accompanied by a downward shift of similar magnitude for the F360 side chain, and the side chains of D362 and I279 side chains showed a 2.5 Å shift (Fig. 5D). Together, the CSP data suggest that hydroxylation of Pio has the greatest effect on the conformation of the ligand entry/exit site and the β-strand region of the PPARγ LBD, but only some of these changes were apparent in the crystal structure.

In addition to providing information about conformational changes via CSP analysis, NMR spectra can offer insight into differences in protein dynamics between two ligand-bound forms. For example, in our differential NMR analysis, a change in NMR lineshape, or peak intensity, indicates a change in dynamics on the microsecond-millisecond (μs-ms) timescale (i.e., intermediate exchange on the NMR timescale between two or more conformations). A number of residues in PioOH-bound PPARγ LBD showed an increase in NMR peak intensity compared to Pio-bound PPARγ LBD, indicating PioOH stabilized μs-ms timescale dynamics introduced by Pio (Fig. 6A–C). Importantly, many of the stabilized residues were located at the AF-2 coactivator binding surface, indicating that PioOH may more effectively stabilize h12 docking against h3 and h11 in the AF-2 “active” conformation that is compatible with coactivator binding.

Whereas NMR lineshape analysis reports on μs-ms timescale dynamics, HDX-MS probes molecular “breathing” motions or dynamics on a timescale of seconds [33]. To determine whether the enhanced AF-2 stabilization observed for PioOH by NMR can be detected at longer timescales, we performed differential HDX-MS of PPARγ LBD bound to Pio or PioOH (Fig. 5A; Table S1). Consistent with our NMR analysis, PioOH afforded greater protection from deuterium exchange than Pio for peptides within h3 and the h3-h4/5 loop, which are structural elements that comprise the AF-2 surface. There was also stabilization of the h6–7 loop region, which exhibited significant NMR CSPs and stabilization of μs-ms time scale dynamics when bound to PioOH, inferred by increased NMR peak intensities. Taken together, the NMR and HDX-MS reveal that PioOH better stabilizes the AF-2 surface.

PioOH differentially affects coregulator binding mechanisms

Although our binding assays showed that PioOH is less potent than Pio, our NMR and HDX-MS analyses revealed that PioOH more effectively stabilizes the AF-2 surface. AF-2 stabilization is linked to enhanced functional agonism through higher affinity coactivator binding [34]. To test this directly, we performed fluorescence polarization (FP) assays to determine how Pio hydroxylation affects the binding affinity of PPARγ LBD for the TRAP220 coactivator peptide. Compared to apo-PPARγ LBD, both ligands increased the affinity of the TRAP220 peptide relative to apo-PPARγ LBD. PioOH-bound PPARγ LBD bound to the TRAP220 coactivator peptide with higher affinity than Pio-bound PPARγ LBD (Fig. 7A).

We also tested the effect of PioOH vs. Pio on corepressor binding affinity. Using FP assays with a FITC-labeled NCoR1 corepressor peptide, we found that both ligands reduced the affinity of the NCoR1 peptide relative to apo-PPARγ LBD (Fig. 7B), but the difference in NCoR1 peptide affinity between Pio- and PioOH-bound PPARγ LBD was not significant (P~0.5). Taken together, this indicates that although the ligand-dependent effects on coactivator and corepressor binding affinities may be related, where TZD agonists both strengthen TRAP220 coactivator affinity and weaken NCoR1 corepressor affinity relative to apo-PPARγ, they are not directly correlated since the ligand that improved TRAP220 coactivator affinity (PioOH) did not have a greater effect on weakening NCoR1 corepressor affinity.

In addition to the enhanced coactivator binding affinity revealed by the FP assay, the polarization window for TRAP220 binding produced by PioOH was greater than that of Pio, suggesting a greater reduction in molecular tumbling or better stabilization of peptide binding, perhaps via better AF-2 stabilization, at saturating conditions. To test the thermodynamic basis of this observation, we performed isothermal titration calorimetry using the unlabeled TRAP220 peptide and the PPARγ LBD bound to two molar equivalents of either Pio or PioOH (Fig. 8A and B). Consistent with the FP assay, the K_d of peptide binding was lower for PioOH-bound PPARγ, but did not achieve statistical significance; however, the enthalpy (ΔH) of binding was significantly reduced compared to Pio, suggesting stabilized electrostatic contacts with TRAP220 when bound to PioOH (Table 6 and Fig. 8C). Additionally, the entropy (ΔS) of binding was more negative and thus less favorable for PioOH, indicating that the binding dynamics between TRAP220 and PioOH-bound PPARγ LBD are less flexible than for the Pio-bound structure.

PioOH enhances the transcriptional activity of the PPARγ LBD

To compare the cellular activation properties of Pio and PioOH, we performed transcriptional reporter assays by transfecting HEK293T cells with an expression plasmid encoding full-length PPARγ along with a reporter plasmid containing three copies of the PPAR DNA response element (3xPPRE) upstream of the luciferase gene. Both Pio and PioOH caused a concentration-dependent increase in PPARγ transcription, and consistent with the biochemical binding data PioOH showed reduced cellular potency relative to Pio (Fig. 9A).

We also performed a cell-based transcriptional reporter assay using a chimeric expression construct comprised of the PPARγ LBD fused to the Gal4 yeast transcription factor DBD. This construct lacks the N-terminal ligand-independent activation function-1 (AF-1) and native DNA-binding domain in PPARγ and thus reports on LBD activity only, and provides a higher window of activation and is therefore more sensitive to graded levels of agonism that correlates well for full vs. partial agonist effects on target gene expression [11] compared to the full-length PPARγ/3xPPRE assay. We transfected HEK293T cells with the Gal4-PPARγ LBD expression plasmid and a reporter plasmid containing five tandem repeats of the Gal4 Upstream Activation Sequence (5xUAS) placed upstream of the luciferase gene. Consistent with the full-length PPARγ results, PioOH was less potent than Pio (Fig. 9B). Intriguingly, however, PioOH yielded a significantly greater maximal luciferase activity than

Pio. Thus, enhanced AF-2 surface stabilization afforded by PioOH corresponds to increased transcriptional activition of the LBD-only construct, which may not be apparent in the full-length assay due to lower sensitivity or contributions of the N-terminal ligand-independent AF-1 domain.

Discussion and Conclusions

Pioglitazone (Pio) remains an important option for treatment of T2DM because of its potent insulin sensitizing effects [35, 36]. However, adverse side effects have warranted further investigation into its *in vivo* mechanism of action. Although it has been reported that some Pio metabolites retain antihyperglycemic effects, albeit with reduced potency [25], to our knowledge, it has not been shown how Pio metabolites, or the metabolites of any other PPARγ-binding drug, affect the structure and function of PPARγ.

Investigating the structure and function of nuclear receptor ligand metabolites has provided essential insight to into the activity of the parent ligand/drug *in vivo*. For example, testosterone is the primary endogenous ligand of androgen receptor (AR), but in tissues expressing 5α-reductase, testosterone is converted to 5α-dihydrotestosterone (5α-DHT), which binds with greater selectivity and affinity to AR and is thought to enhance androgenic effects in specific tissues such as the prostate and seminal vesicles [37]. Intriguingly, 5α-DHT differs from testosterone only by the presence of an additional unsaturated double bond and, similar to our analysis here of PPARγ, crystal structures of AR LBD bound to 5α-DHT or testosterone revealed no overt structural changes (overall Cα rmsd only 0.39 Å, similar to the rmsd between Pio- and PioOH-bound PPARγ LBD) that would lead to improved function [38]. However, comprehensive analysis of atomic geometries within the AR ligand-binding pocket revealed the subtle interactions in the two liganded complexes that determine AR ligand affinity [39]. Thus, seemingly insignificant structural changes can underlie important functional differences.

Under this premise, we performed a comparative structure-function analysis of Pio and its major *in vivo* Pio metabolite, 1-hydroxypioglitazone (PioOH), using X-ray crystallography, *in silico* docking, and solution-state structural methods in combination with biochemical and cell-based assays. We found that PioOH binds PPARγ with weaker affinity than Pio, but produces a modestly more efficacious agonist response at saturating ligand conditions in biochemical (TR-FRET) and cellular (chimeric Gal4 transactivation) assays, potentially due to stabilization of an LBD conformation with enhanced coactivator binding affinity. Crystal structures of PPARγ LBD bound to Pio and PioOH did not show any overall structural changes that could lead to the improved agonist profile of PioOH, but solution-state structural analysis using NMR spectroscopy and HDX-MS revealed that PioOH better stabilizes the dynamics of the AF-2 surface. This is consistent with its improved biochemical, thermodynamic, and cellular agonist effects on PPARγ compared to Pio. The reduced potency of PioOH likely underlies its reduced anti-hyperglycemic efficacy relative to Pio [25, 26], but our results suggest that if PioOH concentrations were higher than Pio, it could be more efficacious.

Structure activity relationship (SAR) analysis of parent drugs is often performed early in drug development [40], and later compound modifications are made to maximize pharmacokinetic (PK) and pharmacodynamic (PD) properties [41]. These studies determine drug metabolite safety and activity, but not their structure and function. Pio PK/PD studies showed that PioOH is an active metabolite with nearly triple the total body exposure of Pio [24], so it could be responsible for a significant portion of Pio's effects, including its negative side effects. It is possible that variations in local tissue concentrations prior to excretion could result in transient saturating PioOH levels. Importantly, the structure-function analysis presented here indicate that this scenario could result in a slight overactivation of PPARγ compared to the parent drug (Pio) if local drug concentrations are high enough.

Our work indicates that the introduction of the water-mediated hydrogen bond between the hydroxyl and the S342 side chain likely underlies the weakened binding affinity of PioOH relative to Pio. This was somewhat unexpected because the hydrogen bonding ability introduced by the addition of the hydroxyl group in PioOH in an otherwise hydrophobic ligand side chain (in Pio) would typically be considered as overall favorable for binding affinity, but underlies the notion that hydrophobic effects also play an important role in ligand binding affinity [42]. However, although PioOH displayed weaker binding affinity than Pio, PioOH better stabilized LBD regions including the AF-2 coregulator surface and a region of helix 7 that includes a ligand-dependent SUMOylation site (K367) implicated in promoting PPARγ-mediated repression of pro-inflammatory genes [43]. The water-mediated hydrogen bond observed between PioOH and S342 side chain in our crystal structure was confirmed by molecular docking and our analysis of chemical shift changes by NMR, which indicated conformational changes for residues within the β-sheet region of the ligand-binding pocket. Ligand interactions with the backbone amide of S342 have previously been implicated in inhibiting the phosphorylation of S273 (S245 in PPARγ isoform 1), which is associated with obesogenic side effects of PPARγ activation [18, 19]. Thus, it will be interesting to determine in future studies if the Pio metabolites, including PioOH, enhance Pio's non-classical effects on PPARγ activity. Together, our findings identify the structural nuances that can underlie a drug's *in vivo* effects and demonstrate the importance of investigating the structural basis of nuclear receptor drug metabolite activity.

Experimental Section

1. Ligands and protein preparation

Pioglitazone (Pio; Cayman Chemical) and 1-hydroxypioglitazone (PioOH; Axon Medchem) were purchased from commercial sources. 100% purity for PioOH was validated by the supplier by HPLC, NMR, and MS. Pio purity was also validated by the supplier: ≥98% by HPLC. Pio and PioOH were prepared in DMSO-d_6 as 50 mM and 7 mM stocks, respectively. Human PPARγ LBD (residues 203–477, isoform 1 numbering) was expressed in *Escherichia coli* BL21(DE3) cells as TEV-cleavable hexahistidine (6xHis)-tagged fusion protein using protocols previously described [11, 12]. Purified protein was delipidated using LIPIDEX 1000 resin (Perkin Elmer) and stored in 20 mM potassium phosphate (pH 7.4), 50 mM potassium chloride, 0.5 mM EDTA, and 5 mM TCEP. FITC-labeled peptides derived from the TRAP220 coactivator (residues 638–656; NTKNHPMLMNLLKDNPAQD) and

NCoR1 corepressor (residues 2256–2278; DPASNLGLEDIIRKALMGSFDDK) were synthesized by Lifetein; peptides contained a six-carbon linker (Ahx) after the FITC label, and the C terminus was amidated for stability.

2. Circular dichroism (CD) spectroscopy

CD wavelength scans and thermal denaturation experiments monitored at 222 nm were performed in CD buffer (10 mM potassium phosphate (pH 7.4) and 50 mM potassium fluoride) to determine the folding and stability of PPARγ LBD (10 μM) in the presence of one molar equivalent of Pio or PioOH on a Jasco J-815 spectropolarimeter. Thermal denaturation was monitored at 1°C intervals along a temperature gradient from 20°C to 80°C. Raw ellipticity was plotted using GraphPad Prism and fit to a set of equations based on the Gibbs-Helmholtz equation, as previously reported [44].

3. TR-FRET competitive ligand displacement and coregulator interaction assays

Time-resolved fluorescence resonance energy transfer (TR-FRET) assays were performed in black low-volume 384-well plate (Greiner) using a buffer containing 20 mM potassium phosphate (pH 7.4), 50 mM potassium chloride, 0.5 mM EDTA, and 5 mM TCEP, and 0.01% Tween-20. For the ligand displacement assay, each well (22.5 μL per well) contained 1 nM 6xHis-PPARγ LBD protein, 1 nM LanthaScreen Elite Tb-anti-His Antibody (Thermo Fisher Scientific), and 5 nM Fluormone Pan-PPAR Green tracer ligand (Invitrogen) in TR-FRET buffer. For the TR-FRET coregulator interaction assay, each well contained 400 nM FITC-labeled TRAP220 or NCoR1 peptides, 4 nM 6xHis-PPARγ LBD protein, 1 nM LanthaScreen Elite Tb-anti-His Antibody (Thermo Fisher Scientific), and 400 nM peptide in TR-FRET buffer in 22.5 μL total volume per well. Ligand stocks were prepared via serial dilution in DMSO, added to wells in triplicate to a final DMSO concentration of 1%, and the plates were incubated at 25 °C for ~1 h and read using BioTek Synergy Neo multimode plate reader. The Tb donor was excited at 340 nm; its fluorescence emission was monitored at 495 nm, and the acceptor FITC emission was measured at 520 nm. The TR-FRET ratio was calculated as the signal at 520 nm divided by the signal at 495 nm. Data were plotted using GraphPad Prism and fit to the appropriate equation: for the ligand displacement assay, data were fit to a competitive one site fit K_i equation using the known binding affinity of Fluormone™ Pan-PPAR Green tracer ligand (2.8 nM; Thermo Fisher Scientific product insert PV4894); and for the coregulator interaction assay data were fit to a sigmoidal dose response equation. For the competitive binding assay, significance was determined by F-test analysis of the Pio vs. PioOH fit Ki value. For the TR-FRET coregulator recruitment assays, significance was determined by unpaired t-test of EC/IC_{50} values from n=2 individual experiments.

4. Cell-based transactivation assays

HEK293T cells (ATCC; cat# CRL-3216) cultured in DMEM media (Gibco) supplemented with 10% fetal bovine serum (FBS) and 50 units mL^{-1} of penicillin, streptomycin, and glutamine were grown to 90% confluency in a T-75 flask before seeding 4 million cells per well in 10-cm dishes. Seeded cells were transfected using transfection reagent containing 27 μL X-treme Gene 9 (Roche) in serum-free Opti-mem reduced serum media (Gibco) with either 4.5 μg pCMV6-XL4 plasmid containing full-length human PPARγ2 and 4.5 μg 3X

multimerized PPRE-luciferase reporter or 4.5 μg Gal4-PPARγ LBD and 4.5 μg 5X Upstream Activation Sequence (UAS) luciferase reporter. After 18 hrs incubation at 37 °C in a 5% CO_2 incubator, the transfected cells were plated in quadruplicate in white 384-well plates (Perkin Elmer) at a density of 10,000 cells per well (20 μL volume) and incubated 4 hrs then treated with 20 μL of vehicle control (1% DMSO in DMEM media) or 1:2 serial dilution of each compound from 56 pM–10 μM (1% final DMSO concentration). After 18 hrs, luciferase activity was measured by addition of 20 μL Britelite Plus (Perkin Elmer) and luminescence was read using a BioTek Synergy Neo multimode plate reader. Data were plotted in GraphPad Prism as fold change in luminescence of compound-treated cells over DMSO-treated control cells vs ligand concentration and fit to a sigmoidal dose response equation. EC_{50} values from n=4 individual experiments for full length PPARγ and n=2 individual experiments for PPARγ-Gal4 were analyzed by unpaired t-test; the response window from individual experiments was analyzed by paired t-test.

5. Fluorescence polarization coregulator interaction assays

Fluorescence polarization assays were performed in black low-volume 384-well plates (Greiner) using a buffer containing 20 mM potassium phosphate (pH 7.4), 50 mM potassium chloride, 0.5 mM EDTA, 5 mM TCEP, and 0.01% Tween-20. Each well contained 100 nM FITC-labeled TRAP220 coactivator peptide (Lifetein), a serial dilution of PPARγ LBD (1.5 nM–90 μM), with a fixed concentration of vehicle control (1% DMSO) or ligand equal to the highest protein concentration (90 μM Pio or PioOH) in triplicate. Plates were incubated 2 hrs at 4°C and read using BioTek Synergy Neo multimode plate reader. Data were plotted in GraphPad Prism and fit to a sigmoidal dose response equation. Peptide affinity and polarization window from n=2 individual experiments was analyzed by unpaired t-test.

6. Isothermal titration calorimetry

A peptide derived from the TRAP220 coactivator (residues 638–656; NTKNHPMLMNLLKDNPAQD) was synthesized by Lifetein and resuspended at 500 μM in buffer containing 20 mM potassium phosphate (pH 7.4), 50 mM potassium chloride, 0.5 mM EDTA, and 5 mM TCEP. PPARγ LBD was prepared at 50 μM in identical buffer. 100 μM Pio or PioOH were added to PPARγ LBD and TRAP220 and incubated on ice 30 minutes before each experiment. TRAP220 peptide (syringe) was titrated into PPARγ LBD (sample cell). 20 total injections were made per experiment (0.4 μL for the first injection, 2.0 μL for subsequent injections), using a mixing speed of 1200 rpm, a reference power of 5 μcal/second, and a cell temperature of 25ºC. Two runs were performed for each ligand-bound condition. Experiments were performed using a MicroCal iTC200 (Malvern). Data were processed in NITPIC [45] to determine binding stoichiometry and further analyzed by unbiased global fitting of both replicate runs per ligand-bound condition in SEDPHAT [46], followed by export to GUSSI for publication-quality figure preparation [47]. The SEDPHAT fitting model used was A + B to AB heteroassociation and the fit parameters were enthalpy (ΔH) and affinity (K_d).

7. NMR spectroscopy

Two dimensional [^{1}H,^{15}N] -transverse relaxation optimized spectroscopy (TROSY)-heteronuclear single quantum correlation (HSQC) data were collected at 298K using a

Bruker 700 Mhz NMR instrument equipped with a QCI cryoprobe. Samples contained 200 μM ^{15}N-labeled PPARγ LBD in a buffer (NMR buffer) containing 20 mM potassium phosphate (pH 7.4), 50 mM potassium chloride, 0.5 mM EDTA, 5 mM TCEP, and 10% D_2O in the absence or presence of two molar equivalents of Pio or PioOH. Data were processed and analyzed using Topspin 3.0 (Bruker) and NMRViewJ (OneMoon Scientific, Inc.) [48]. NMR analysis was performed using previously described rosiglitazone-bound NMR chemical shift assignments (BMRB entry 17975) for well resolved residues with consistent NMR peak positions via the minimum chemical shift procedure [11, 31].

8. X-ray crystallography

PPARγ LBD was incubated with 1-hydroxypioglitazone at a 1:3 protein/ligand molar ratio in PBS overnight before being concentrated to 10 mg/ml. Crystals were obtained after 7–10 days at 22°C by sitting-drop vapor diffusion against 50 μL of well solution. The crystallization drops contain 1 μL of protein sample mixed with 1 μL of reservoir solution containing 0.1 M Tris-HCl, 0.8 M sodium citrate at pH 7.6. Crystals were flash-cooled in liquid nitrogen before data collection. Data collection was carried out at Beamline 5.0.2 at Berkeley Center for Structural Biology (Advanced Light Source). Data were processed, integrated, and scaled with the programs Mosflm and Scala in CCP4 [49, 50]. The structure was solved at 1.88Å by molecular replacement using the program Phaser [51] that was implemented in the PHENIX package [52] using a previously published PPARγ LBD crystal structure (PDB code: 1PRG [53]) as the search model. The structure was refined using PHENIX with several cycles of interactive model rebuilding in COOT [54].

9. Hydrogen/deuteirum exchange mass spectrometry (HDX-MS)

Solution-phase amide HDX experiments were carried out with a fully automated system described previously [55] with slight modifications. Five μl of PPARγ LBD protein (10 μM), without or with Pio or PioOH (100 μM), was mixed with 20 μL of D_2O-containing NMR buffer and incubated at 4 °C for a range of time points (0s, 10s, 30s, 60s, 900s or 3,600s). Following exchange, unwanted forward or back exchange was minimized and the protein was denatured with a quench solution (5 M urea, 50 mM TCEP and 1% v/v TFA) at 1:1 ratio to protein. Samples were then passed through an in-house prepared immobilized pepsin column at 50 μL min^{-1} (0.1% v/v TFA, 15 °C) and the resulting peptides were trapped on a C_{18} trap column (Hypersil Gold, Thermo Fisher). The bound peptides were then gradient-eluted (5–50% CH_3CN w/v and 0.3% w/v formic acid) across a 1 mm × 50 mm C_{18} HPLC column (Hypersil Gold, Thermo Fisher) for 5 min at 4 °C. The eluted peptides were then analyzed directly using a high resolution Orbitrap mass spectrometer (Q Exactive, Thermo Fisher). Each HDX experiment was performed in triplicate. To identify peptides, MS/MS experiments were performed with a Q Exactive mass spectrometer over a 70 min gradient. Product ion spectra were acquired in a data-dependent mode and the five most abundant ions were selected for the product ion analysis. The MS/MS *.raw data files were converted to *.mgf files and then submitted to Mascot (Matrix Science, London, UK) for peptide identification. Peptides with a Mascot score of 20 or greater were included in the peptide set used for HDX detection. The MS/MS Mascot search was also performed against a decoy (reverse) sequence and false positives were ruled out. The MS/MS spectra of all the peptide ions from the Mascot search were further manually inspected and only the unique charged

ions with the highest Mascot score were used in estimating the sequence coverage. The intensity weighted average m/z value (centroid) of each peptide isotopic envelope was calculated with the latest version of our in-house developed software, HDX Workbench [56].

10. Molecular Docking

The PPARγ metabolites, including Pio and PioOH, were prepared from SMILES strings using OpenBabel (MMFF94s forcefield; SD/CG minimization), enumerating all stereogenic center conformations, for a total of 18 different ligands. For the receptor, chain A was considered for the docking, hydrogens were added with REDUCE [57], then the standard AutoDock protocol was followed for the preparation [58]. To investigate the potential role of water molecules in ligand binding, dockings were performed without any crystallographic waters, then including those interacting directly with the ligand PioOH in the crystallographic structures: HOH709 alone, HOH628–692 alone, and HOH709 and HOH628–692 together. Docking were performed using AutoDock Vina [59]. The docking search space was centered around the position of the co-crystallized ligand from chain A, 1-hydroxypioglitazone (PioOH), in the PPARγ LBD (PDB code 6DH9) with each dimension extended 22.5 Å from the ligand. Dockings were performed with standard search parameters and poses with the best score were selected for the analysis.

Supplementary Material

Refer to Web version on PubMed Central for supplementary material.

Acknowledgements

This work was supported by National Institutes of Health (NIH) grants R01DK101871 (DJK), R01DK105825 (PRG), F32DK108442 (RB), and GM069832 (SF); National Science Foundation (NSF) funding to the Summer Undergraduate Research Fellows (SURF) program at Scripps Research [Grant 1659594]; and the Academic Year Research Internship for Undergraduates (AYRIU) program at Scripps Research.

Abbreviations

AF-1	activation function-1
AF-2	activation function-2
CSP	chemical shift perturbation
DBD	DNA-binding domain
HDX-MS	hydrogen/deuterium exchange mass spectrometry
LBD	ligand-binding domain
NCoR1	Nuclear Receptor Corepressor 1
Pio	pioglitazone
PioOH	1-hydroxypioglitazone
PPRE	PPAR response element

TRAP220	Thyroid hormone Receptor Associated Protein 220
TZD	thiazolidinedione

References

1. Guan HP; Ishizuka T; Chui PC; Lehrke M; Lazar MA Corepressors Selectively Control the Transcriptional Activity of PPARgamma in Adipocytes. Genes Dev 2005, 19, 453–461. [PubMed: 15681609]
2. Ahmadian M; Suh JM; Hah N; Liddle C; Atkins AR; Downes M; Evans RM PPARgamma Signaling and Metabolism: The Good, the Bad and the Future. Nat Med 2013, 19, 557–566. [PubMed: 23652116]
3. Moore JT; Collins JL; Pearce KH The Nuclear Receptor Superfamily and Drug Discovery. ChemMedChem 2006, 1, 504–523. [PubMed: 16892386]
4. Tugwood JD; Issemann I; Anderson RG; Bundell KR; McPheat WL; Green S The Mouse Peroxisome Proliferator Activated Receptor Recognizes a Response Element in the 5' Flanking Sequence of the Rat Acyl Coa Oxidase Gene. EMBO J 1992, 11, 433–439. [PubMed: 1537328]
5. Helledie T; Grontved L; Jensen SS; Kiilerich P; Rietveld L; Albrektsen T; Boysen MS; Nohr J; Larsen LK; Fleckner J; Stunnenberg HG; Kristiansen K; Mandrup S The Gene Encoding the Acyl-Coa-Binding Protein Is Activated by Peroxisome Proliferator-Activated Receptor gamma through an Intronic Response Element Functionally Conserved between Humans and Rodents. J Biol Chem 2002, 277, 26821–26830. [PubMed: 12015306]
6. Meijsing SH; Pufall MA; So AY; Bates DL; Chen L; Yamamoto KR DNA Binding Site Sequence Directs Glucocorticoid Receptor Structure and Activity. Science (New York, N.Y.) 2009, 324, 407–410.
7. de Vera IMS; Zheng J; Novick S; Shang J; Hughes TS; Brust R; Munoz-Tello P; Gardner WJ Jr.; Marciano DP; Kong X; Griffin PR; Kojetin DJ Synergistic Regulation of Coregulator/Nuclear Receptor Interaction by Ligand and DNA. Structure 2017, 25, 1506–1518.e1504. [PubMed: 28890360]
8. Moore TW; Mayne CG; Katzenellenbogen JA Minireview: Not Picking Pockets: Nuclear Receptor Alternate-Site Modulators (NRAMs). Mol Endocrinol 2010, 24, 683–695. [PubMed: 19933380]
9. Nolte RT; Wisely GB; Westin S; Cobb JE; Lambert MH; Kurokawa R; Rosenfeld MG; Willson TM; Glass CK; Milburn MV Ligand Binding and Co-Activator Assembly of the Peroxisome Proliferator-Activated Receptor-gamma. Nature 1998, 395, 137–143. [PubMed: 9744270]
10. Millard CJ; Watson PJ; Fairall L; Schwabe JW An Evolving Understanding of Nuclear Receptor Coregulator Proteins. J Mol Endocrinol 2013, 51, T23–36. [PubMed: 24203923]
11. Hughes TS; Chalmers MJ; Novick S; Kuruvilla DS; Chang MR; Kamenecka TM; Rance M; Johnson BA; Burris TP; Griffin PR; Kojetin DJ Ligand and Receptor Dynamics Contribute to the Mechanism of Graded PPARγ Agonism. Structure 2012, 20, 139–150. [PubMed: 22244763]
12. Hughes TS; Giri PK; de Vera IMS; Marciano DP; Kuruvilla DS; Shin Y; Blayo A-L; Kamenecka TM; Burris TP; Griffin PR; Kojetin DJ An Alternate Binding Site for PPARγ Ligands. Nat Commun 2014, 5, 3571. [PubMed: 24705063]
13. Ge K; Guermah M; Yuan CX; Ito M; Wallberg AE; Spiegelman BM; Roeder RG Transcription Coactivator TRAP220 Is Required for PPAR gamma 2-Stimulated Adipogenesis. Nature 2002, 417, 563–567. [PubMed: 12037571]
14. Nagy L; Schwabe JWR Mechanism of the Nuclear Receptor Molecular Switch. Trends Biochem Sci 2004, 29, 317–324. [PubMed: 15276186]
15. Marciano DP; Kuruvilla DS; Boregowda SV; Asteian A; Hughes TS; Garcia-Ordonez R; Corzo CA; Khan TM; Novick SJ; Park H; Kojetin DJ; Phinney DG; Bruning JB; Kamenecka TM; Griffin PR Pharmacological Repression of PPARgamma Promotes Osteogenesis. Nat Commun 2015, 6, 7443. [PubMed: 26068133]
16. Bruning JB; Chalmers MJ; Prasad S; Busby SA; Kamenecka TM; He Y; Nettles KW; Griffin PR Partial Agonists Activate PPARgamma Using a Helix 12 Independent Mechanism. Structure 2007, 15, 1258–1271. [PubMed: 17937915]

17. Hughes TS; Shang J; Brust R; de Vera IMS; Fuhrmann J; Ruiz C; Cameron MD; Kamenecka TM; Kojetin DJ Probing the Complex Binding Modes of the PPARγ Partial Agonist 2-Chloro-N-(3-Chloro-4-((5-Chlorobenzo[D]Thiazol-2-Yl)Thio)Phenyl)-4-(Trifluoromethyl)Benzenesulfonamide (T2384) to Orthosteric and Allosteric Sites with NMR Spectroscopy. J Med Chem 2016, 59, 10335–10341. [PubMed: 27783520]

18. Choi JH; Banks AS; Estall JL; Kajimura S; Bostrom P; Laznik D; Ruas JL; Chalmers MJ; Kamenecka TM; Bluher M; Griffin PR; Spiegelman BM Anti-Diabetic Drugs Inhibit Obesity-Linked Phosphorylation of PPARgamma by Cdk5. Nature 2010, 466, 451–456. [PubMed: 20651683]

19. Choi JH; Banks AS; Kamenecka TM; Busby SA; Chalmers MJ; Kumar N; Kuruvilla DS; Shin Y; He Y; Bruning JB; Marciano DP; Cameron MD; Laznik D; Jurczak MJ; Schurer SC; Vidovic D; Shulman GI; Spiegelman BM; Griffin PR Antidiabetic Actions of a Non-Agonist PPARgamma Ligand Blocking Cdk5-Mediated Phosphorylation. Nature 2011, 477, 477–481. [PubMed: 21892191]

20. Lee MA; Tan L; Yang H; Im Y-G; Im YJ Structures of PPARγ Complexed with Lobeglitazone and Pioglitazone Reveal Key Determinants for the Recognition of Antidiabetic Drugs. Sci Rep 2017, 7, 16837. [PubMed: 29203903]

21. Lehrke M; Lazar MA The Many Faces of PPARgamma. Cell 2005, 123, 993–999. [PubMed: 16360030]

22. Alvarez-Sánchez R; Montavon F; Hartung T; Pähler A Thiazolidinedione Bioactivation: A Comparison of the Bioactivation Potentials of Troglitazone, Rosiglitazone, and Pioglitazone Using Stable Isotope-Labeled Analogues and Liquid Chromatography Tandem Mass Spectrometry. Chem Res Toxicol 2006, 19, 1106–1116. [PubMed: 16918252]

23. Jaakkola T; Laitila J; Neuvonen PJ; Backman JT Pioglitazone Is Metabolised by CYP2C8 and Cyp3a4 in Vitro: Potential for Interactions with CYP2C8 Inhibitors. Basic Clin Pharmacol Toxicol 2006, 99, 44–51. [PubMed: 16867170]

24. Eckland DA; Danhof M Clinical Pharmacokinetics of Pioglitazone. Exp Clin Endocrinol Diabetes 2000, 108, 234–242.

25. Krieter PA; Colletti AE; Doss GA; Miller RR Disposition and Metabolism of the Hypoglycemic Agent Pioglitazone in Rats. Drug Metabolism and Disposition 1994, 22, 625–630. [PubMed: 7956739]

26. Tanis SP; Parker TT; Colca JR; Fisher RM; Kletzein RF Synthesis and Biological Activity of Metabolites of the Antidiabetic, Antihyperglycemic Agent Pioglitazone. J Med Chem 1996, 39, 5053–5063. [PubMed: 8978836]

27. Abdellatif KRA; Fadaly WAA; Kamel GM; Elshaier YAMM; El-Magd MA Design, Synthesis, Modeling Studies and Biological Evaluation of Thiazolidine Derivatives Containing Pyrazole Core as Potential Anti-Diabetic PPAR-Γ Agonists and Anti-Inflammatory Cox-2 Selective Inhibitors. Bioorganic chemistry 2019, 82, 86–99. [PubMed: 30278282]

28. Naim MJ; Alam MJ; Nawaz F; Naidu VGM; Aaghaz S; Sahu M; Siddiqui N; Alam O Synthesis, Molecular Docking and Anti-Diabetic Evaluation of 2,4-Thiazolidinedione Based Amide Derivatives. Bioorganic chemistry 2017, 73, 24–36. [PubMed: 28582649]

29. Parks DJ; Tomkinson NC; Villeneuve MS; Blanchard SG; Willson TM Differential Activity of Rosiglitazone Enantiomers at PPAR gamma. Bioorg Med Chem Lett 1998, 8, 3657–3658. [PubMed: 9934490]

30. Hughes TS; Chalmers MJ; Novick S; Kuruvilla DS; Chang MR; Kamenecka TM; Rance M; Johnson BA; Burris TP; Griffin PR; Kojetin DJ Ligand and Receptor Dynamics Contribute to the Mechanism of Graded PPAR-gamma Agonism. Structure 2012, 20, 139–150. [PubMed: 22244763]

31. Williamson MP Using Chemical Shift Perturbation to Characterise Ligand Binding. Prog Nucl Magn Reson Spectrosc 2013, 73, 1–16. [PubMed: 23962882]

32. Edman K; Hosseini A; Bjursell MK; Aagaard A; Wissler L; Gunnarsson A; Kaminski T; Köhler C; Bäckström S; Jensen TJ; Cavallin A; Karlsson U; Nilsson E; Lecina D; Takahashi R; Grebner C; Geschwindner S; Lepistö M; Hogner AC; Guallar V Ligand Binding Mechanism in Steroid Receptors: From Conserved Plasticity to Differential Evolutionary Constraints. Structure 2015, 23, 2280–2290. [PubMed: 26602186]

33. Konermann L; Pan J; Liu YH Hydrogen Exchange Mass Spectrometry for Studying Protein Structure and Dynamics. Chem Soc Rev 2011, 40, 1224–1234. [PubMed: 21173980]
34. Kojetin DJ; Burris TP Small Molecule Modulation of Nuclear Receptor Conformational Dynamics: Implications for Function and Drug Discovery. Mol Pharmacol 2013, 83, 1–8. [PubMed: 22869589]
35. Schernthaner G; Currie CJ; Schernthaner G-H Do We Still Need Pioglitazone for the Treatment of Type 2 Diabetes? A Risk-Benefit Critique in 2013. Diabetes Care 2013, 36, S155–S161. [PubMed: 23882041]
36. Raz I Guideline Approach to Therapy in Patients with Newly Diagnosed Type 2 Diabetes. Diabetes Care 2013, 36, S139–S144. [PubMed: 23882038]
37. Gao W; Bohl CE; Dalton JT Chemistry and Structural Biology of Androgen Receptor. Chem Rev 2005, 105, 3352–3370. [PubMed: 16159155]
38. Pereira de Jésus-Tran K; Côté P-L; Cantin L; Blanchet J; Labrie F; Breton R Comparison of Crystal Structures of Human Androgen Receptor Ligand-Binding Domain Complexed with Various agonists Reveals Molecular Determinants Responsible for Binding Affinity. Protein Sci 2006, 15, 987–999. [PubMed: 16641486]
39. Ostrowski J; Kuhns JE; Lupisella JA; Manfredi MC; Beehler BC; Krystek JSR; Bi Y; Sun C; Seethala R; Golla R; Sleph PG; Fura A; An Y; Kish KF; Sack JS; Mookhtiar KA; Grover GJ; Hamann LG Pharmacological and X-Ray Structural Characterization of a Novel Selective Androgen Receptor Modulator: Potent Hyperanabolic Stimulation of Skeletal Muscle with Hypostimulation of Prostate in Rats. Endocrinology 2007, 148, 4–12. [PubMed: 17008401]
40. Hughes JP; Rees S; Kalindjian SB; Philpott KL Principles of Early Drug Discovery. Br J Pharmacol 2011, 162, 1239–1249. [PubMed: 21091654]
41. Zhang Z; Tang W Drug Metabolism in Drug Discovery and Development. Acta Pharmaceutica Sinica B 2018, 8, 721–732. [PubMed: 30245961]
42. Snyder PW; Mecinović J; Moustakas DT; Thomas SW; Harder M; Mack ET; Lockett MR; Héroux A; Sherman W; Whitesides GM Mechanism of the Hydrophobic Effect in the Biomolecular Recognition of Arylsulfonamides by Carbonic Anhydrase. Proc Natl Acad Sci U S A 2011, 108, 17889–17894. [PubMed: 22011572]
43. Pascual G; Fong AL; Ogawa S; Gamliel A; Li AC; Perissi V; Rose DW; Willson TM; Rosenfeld MG; Glass CK A SUMOylation-Dependent Pathway Mediates Transrepression of Inflammatory Response Genes by PPAR-gamma. Nature 2005, 437, 759–763. [PubMed: 16127449]
44. Morrison EA; Sanchez JC; Ronan JL; Farrell DP; Varzavand K; Johnson JK; Gu BX; Crabtree GR; Musselman CA DNA Binding Drives the Association of BRG1/hBRM Bromodomains with Nucleosomes. Nat Commun 2017, 8, 16080. [PubMed: 28706277]
45. Keller S; Vargas C; Zhao H; Piszczek G; Brautigam CA; Schuck P High-Precision Isothermal Titration Calorimetry with Automated Peak Shape Analysis. Anal Chem 2012, 84, 5066–5073. [PubMed: 22530732]
46. Brautigam CA; Zhao H; Vargas C; Keller S; Schuck P Integration and Global Analysis of Isothermal Titration Calorimetry Data for Studying Macromolecular Interactions. Nat Protoc 2016, 11, 882. [PubMed: 27055097]
47. Brautigam CA Calculations and Publication-Quality Illustrations for Analytical Ultracentrifugation Data. Methods Enzymol 2015, 562, 109–133. [PubMed: 26412649]
48. Johnson BA Using NMRView to Visualize and Analyze the NMR Spectra of Macromolecules. Methods Mol Biol 2004, 278, 313–352. [PubMed: 15318002]
49. Battye TG; Kontogiannis L; Johnson O; Powell HR; Leslie AG iMOSFLM: A New Graphical Interface for Diffraction-Image Processing with MOSFLM. Acta Crystallogr D Biol Crystallogr 2011, 67, 271–281. [PubMed: 21460445]
50. Winn MD; Ballard CC; Cowtan KD; Dodson EJ; Emsley P; Evans PR; Keegan RM; Krissinel EB; Leslie AG; McCoy A; McNicholas SJ; Murshudov GN; Pannu NS; Potterton EA; Powell HR; Read RJ; Vagin A; Wilson KS Overview of the CCP4 Suite and Current Developments. Acta Crystallogr D Biol Crystallogr 2011, 67, 235–242. [PubMed: 21460441]
51. McCoy AJ; Grosse-Kunstleve RW; Adams PD; Winn MD; Storoni LC; Read RJ Phaser Crystallographic Software. J Appl Crystallogr 2007, 40, 658–674. [PubMed: 19461840]

52. Adams PD; Afonine PV; Bunkoczi G; Chen VB; Echols N; Headd JJ; Hung LW; Jain S; Kapral GJ; Grosse Kunstleve RW; McCoy AJ; Moriarty NW; Oeffner RD; Read RJ; Richardson DC; Richardson JS; Terwilliger TC; Zwart PH The Phenix Software for Automated Determination of Macromolecular Structures. Methods 2011, 55, 94–106. [PubMed: 21821126]

53. Nolte RT, Wisely GB, Westin S, Cobb JE, Lambert MH, Kurokawa R, Rosenfeld MG, Willson TM, Glass CK and Milburn MV Ligand Binding and Co-Activator Assembly of the Peroxisome Proliferator-Activated Receptor-Γ. Nature 1988, 395, 137–143.

54. Emsley P; Cowtan K Coot: Model-Building Tools for Molecular Graphics. Acta Crystallogr D Biol Crystallogr 2004, 60, 2126–2132. [PubMed: 15572765]

55. Chalmers MJ; Busby SA; Pascal BD; He Y; Hendrickson CL; Marshall AG; Griffin PR Probing Protein Ligand Interactions by Automated Hydrogen/Deuterium Exchange Mass Spectrometry. Anal Chem 2006, 78, 1005–1014. [PubMed: 16478090]

56. Pascal BD; Willis S; Lauer JL; Landgraf RR; West GM; Marciano D; Novick S; Goswami D; Chalmers MJ; Griffin PR HDX Workbench: Software for the Analysis of H/D Exchange MS Data. J Am Soc Mass Spectrom 2012, 23, 1512–1521. [PubMed: 22692830]

57. Word JM; Lovell SC; Richardson JS; Richardson DC Asparagine and Glutamine: Using Hydrogen Atom Contacts in the Choice of Side-Chain Amide Orientation. J Mol Biol 1999, 285, 1735–1747. [PubMed: 9917408]

58. Forli S; Huey R; Pique ME; Sanner MF; Goodsell DS; Olson AJ Computational Protein-Ligand Docking and Virtual Drug Screening with the AutoDock Suite. Nat Protoc 2016, 11, 905–919. [PubMed: 27077332]

59. Trott O; Olson AJ AutoDock Vina: Improving the Speed and Accuracy of Docking with a New Scoring Function, Efficient Optimization, and Multithreading. J Comput Chem 2010, 31, 455–461. [PubMed: 19499576]

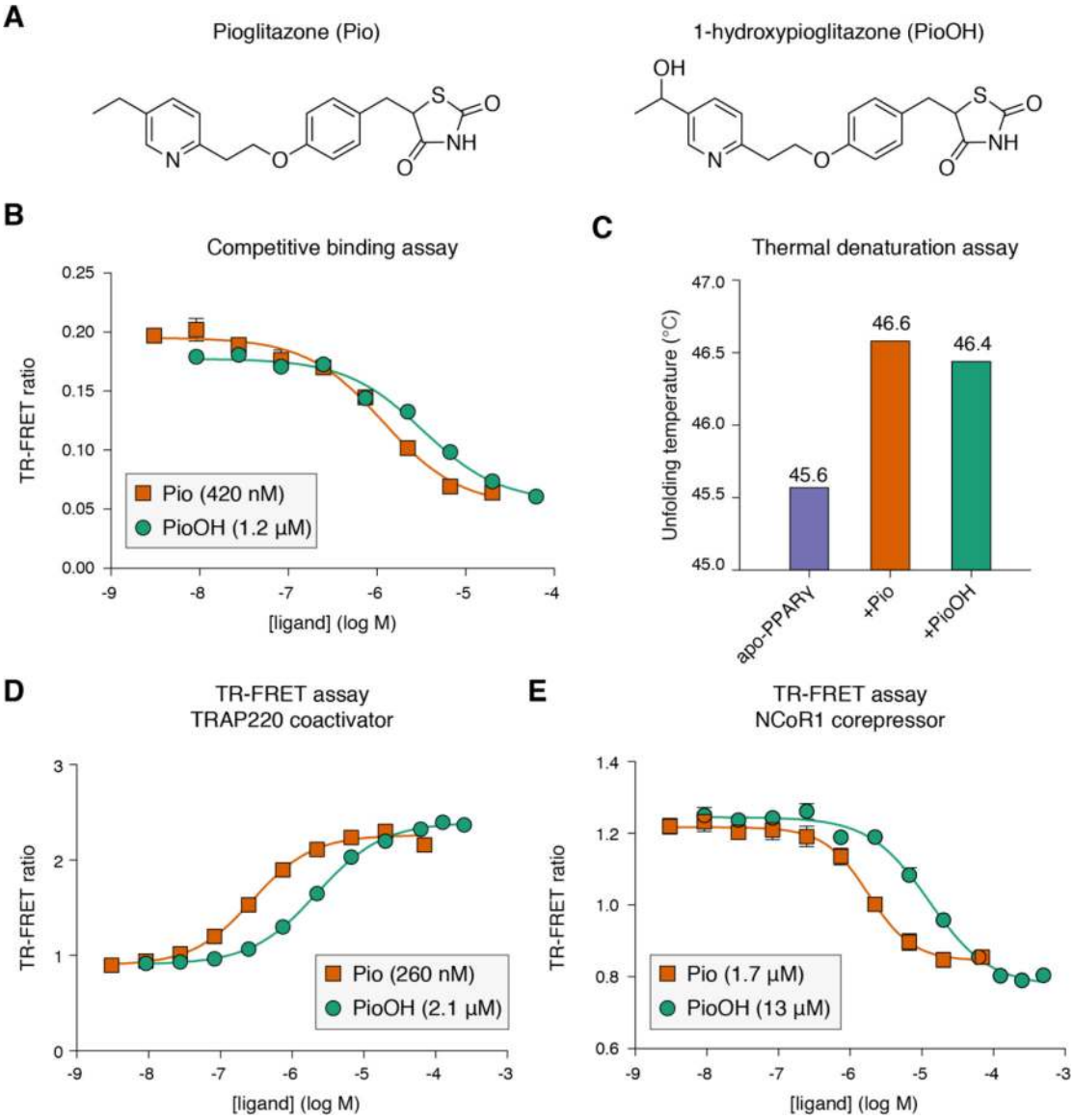

Figure 1.

Functional comparison of Pio and PioOH in biochemical assays. (A) Chemical structures of pioglitazone (Pio; left) and the pioglitazone metabolite 1-hydroxypioglitazone (PioOH; right). (B) Competitive binding assay of PPARγ LBD with titration of Pio or PioOH. Ligand K_i values for Fluormone™ Pan-PPAR displacement are shown in the legend; 95% confidence intervals (CI) are 300–590 nM (Pio) and 0.88–1.6 μM (PioOH) ($P<0.001$). (C) Unfolding temperatures (T_m values) from CD spectroscopy thermal denaturation analysis of delipidated apo-PPARγ LBD without or with addition of ligand. T_m values are noted above the bars; 95% CI are 45.5–45.7°C (apo), 46.4–46.8°C (+Pio), and 46.3–46.6°C (+PioOH). (D) TR-FRET assay of PPARγ LBD with FITC-TRAP220 peptide with Pio or PioOH. Ligand EC_{50} values for peptide recruitment are shown in the legend; average EC_{50} of independent experiments are 260 ± 6 nM (Pio) and 2.1 ± 0.05 μM (PioOH) ($P<0.01$). (E) TR-FRET of PPARγ LBD with FITC-NCoR1 peptide titrated with Pio or PioOH. Ligand

IC_{50} values for peptide displacement are shown in the legend; average EC_{50} of independent experiments are 1.6 ± 0.08 μM (Pio) and 13 ± 1.2 μM (PioOH) ($P<0.05$).

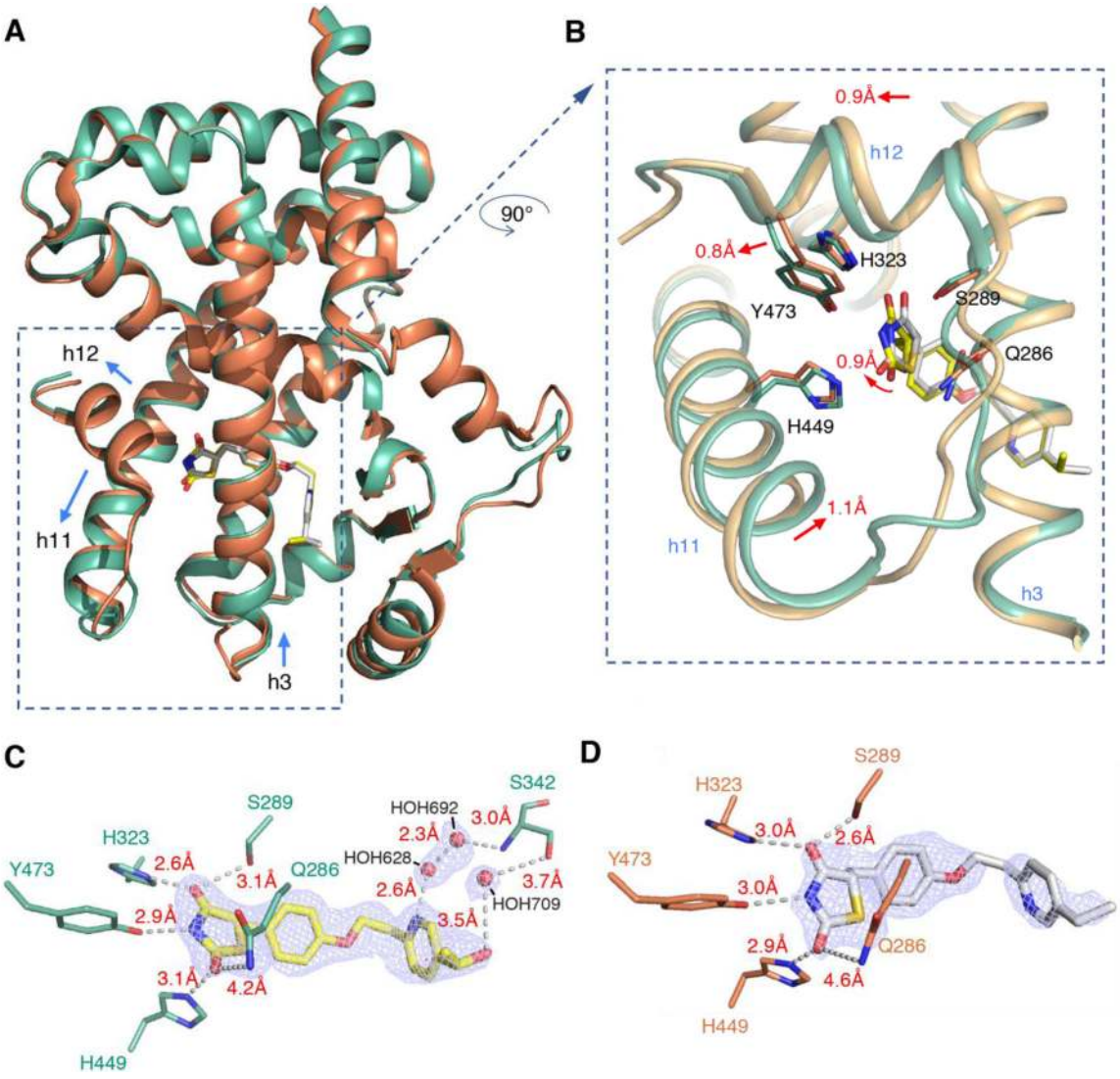

Figure 2.

Comparison of PPARγ LBD crystal structures bound to Pio or PioOH. (A) Structural alignment of PioOH-bound PPARγ LBD crystal structure (PDB code 6DHA, chain A; green cartoon, yellow ligand) and Pio-bound PPARγ LBD crystal structure (PDB code 5Y2O, chain A; orange cartoon, white ligand). (B) 90° counter-clockwise rotation and zoomed in view of the region of the ligand-binding pocket that contacts the Pio and PioOH TZD head groups. The side chains of residues that form hydrogen bonds with TZD head group are shown as sticks, and red arrows indicate structural shifts in secondary structure between the Pio and PioOH-bound structures. (C,D) Omit maps ($2F_O–F_C$, contoured at 1 σ) of (C) PioOH and (D) Pio displayed with hydrogen bonds to residues within the ligand-binding pocket (gray dotted line and red text), as well as water molecules (red spheres) in the PioOH structure including HOH709, which participates in a water-mediated hydrogen bond between the S342 side chain and the PioOH hydroxyl group, and HOH628/HOH692, which participate in a water-mediated hydrogen bond between the PioOH pyridinyl nitrogen and the S342 backbone nitrogen (C).

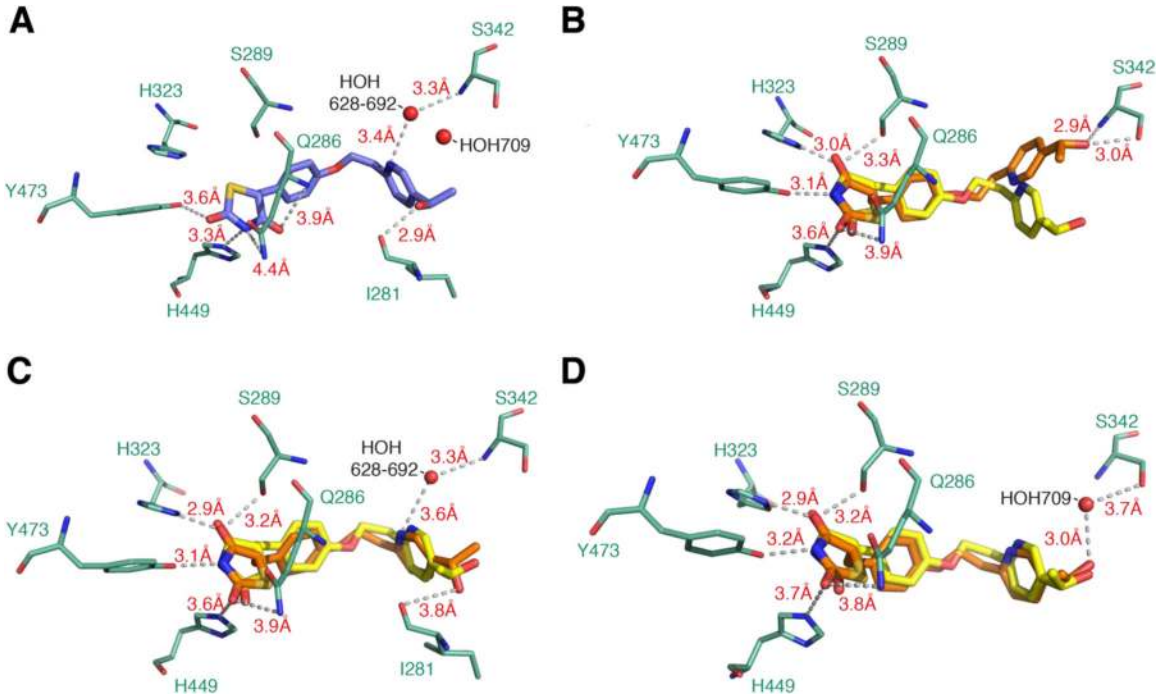

Figure 3.

Effects of ligand stereochemistry and water-mediated hydrogen bonds analyzed by molecular docking. (A) (*R, R*)-PioOH (slate) docked into the (*S, S*)-PioOH-bound PPARγ LBD structure (green) exhibits altered hydrogen bonding interactions. HOH709 and HOH628–692 are indicated with red spheres and bond distances are shown by gray dashes with red text labels. (B) X-ray (*S, S*)-PioOH (yellow) compared to (*S, S*)-PioOH (orange) docked without waters included reveals a large shift in the tail, including a pyridinyl ring flip directing the nitrogen inward toward the ligand binding pocket. (C) X-ray (*S, S*)-PioOH (yellow) compared to (*S, S*)-PioOH (orange) docked with only HOH628–692 included improves the binding mode, but the 1-hydroxyl directs toward I281 on H3 unless HOH709 is included in the docking procedure, as is shown in (D).

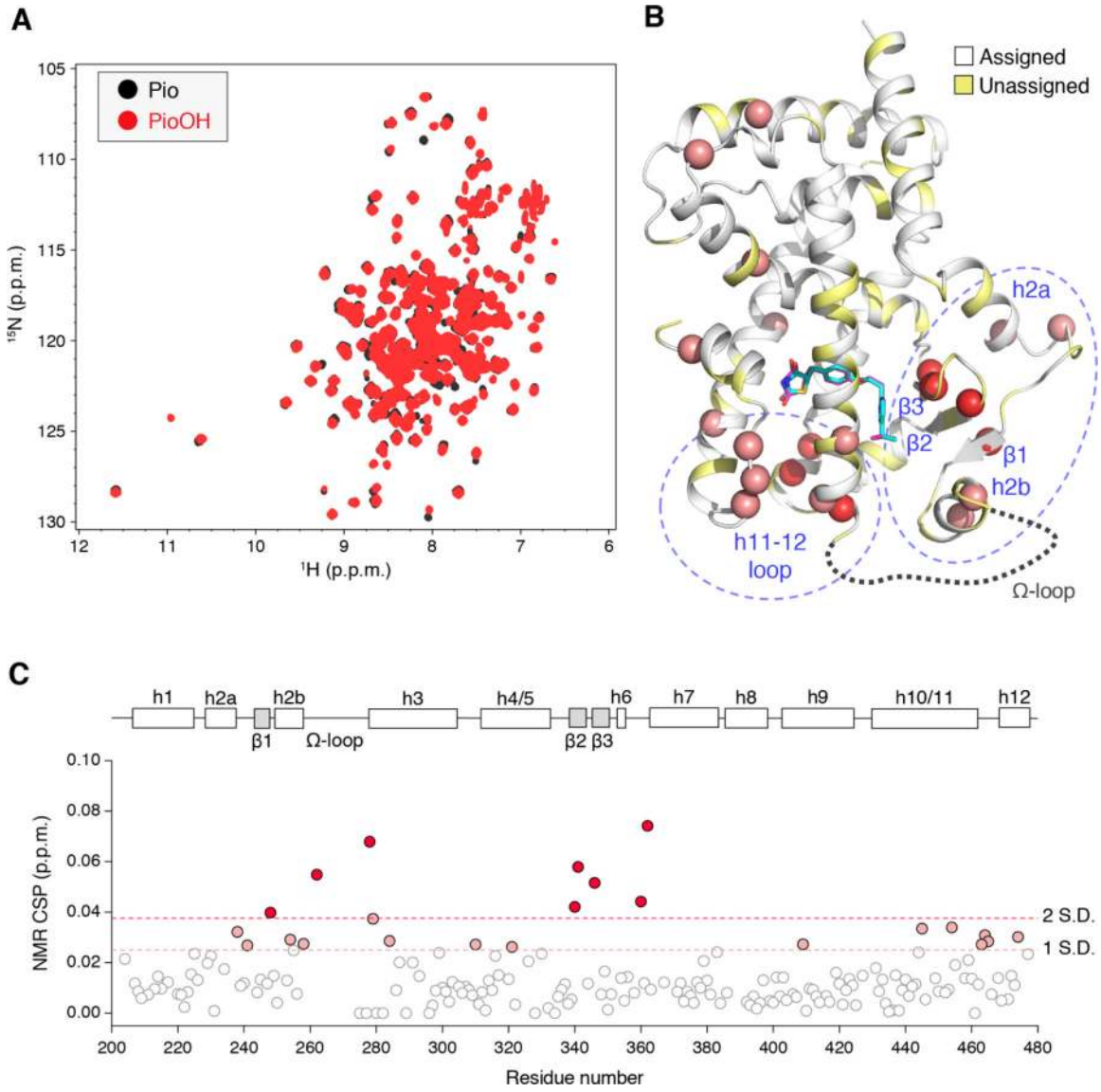

Figure 4.

Differential NMR analysis of Pio- and PioOH-bound PPARγ LBD. (A) Overlay of 2D [^{1}H, ^{15}N]-TROSY-HSQC spectra ^{15}N-labeled PPARγ LBD (200 μM) with 2 molar equivalents of Pio or PioOH. (B) Residues with NMR chemical shift perturbations (CSPs) greater than 1 S.D. from the average plotted on the PPARγ LBD with the Pio and PioOH ligands displayed as blue and magenta sticks, respectively. Blue dashed ovals indicate two regions with the most CSPs, the β-sheet region and the putative pocket entry/exit region. The dashed gray loop indicates the conformationally flexible Ω-loop absent from in the crystal structures. Pio is shown in light blue and PioOH is shown in magenta. (C) NMR CSPs plotted by residue; residues are highlighted with CSPs > 1 S.D. (pink dashed lines and circles) or 2 S.D. (red dashed line and circles) from the mean CSP (0.013 p.p.m.). PPARγ LBD structural elements are depicted linearly above the graph.

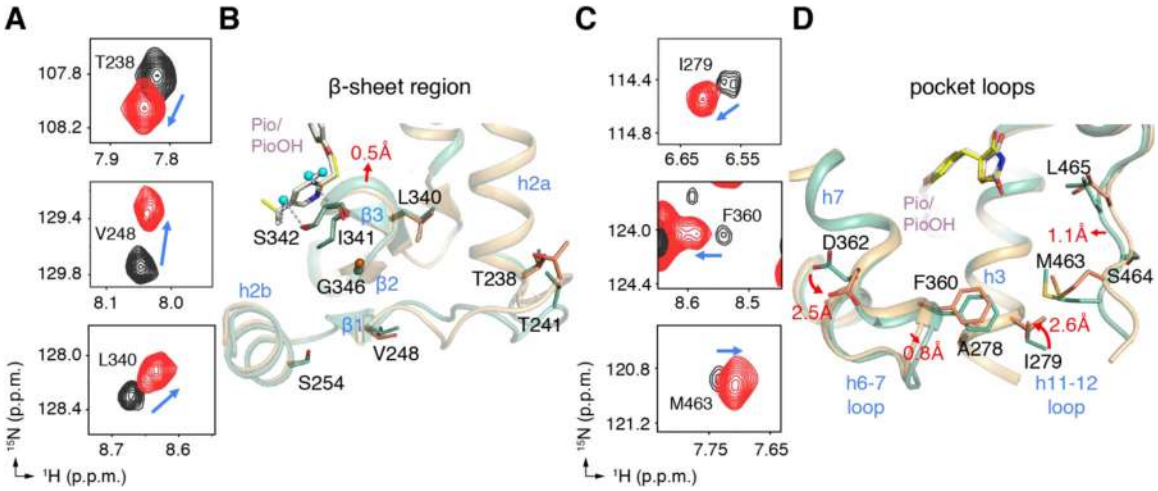

Figure 5.

Correlation between differential NMR data and crystal structures. (A) Representative residues with notable NMR CSPs in the β-sheet region of the ligand-binding pocket. Blue arrows indicate the direction of the CSP from Pio (black peaks) to PioOH (red peaks). (B) Subtle conformational changes in β-strand region are observed in PPARγ LBD crystal structures bound to Pio (PDB code 5Y2O, chain A; light orange cartoon, white ligand) and PioOH (PDB code 6DHA, chain A; light green cartoon, yellow ligand; waters shown as cyan spheres). (C) Representative residues, depicted as in (A), with notable CSPs in the ligand entry/exit region of the ligand-binding pocket, which (D) also manifest as subtle conformational changes in ligand-bound crystal structures, as depicted in (B).

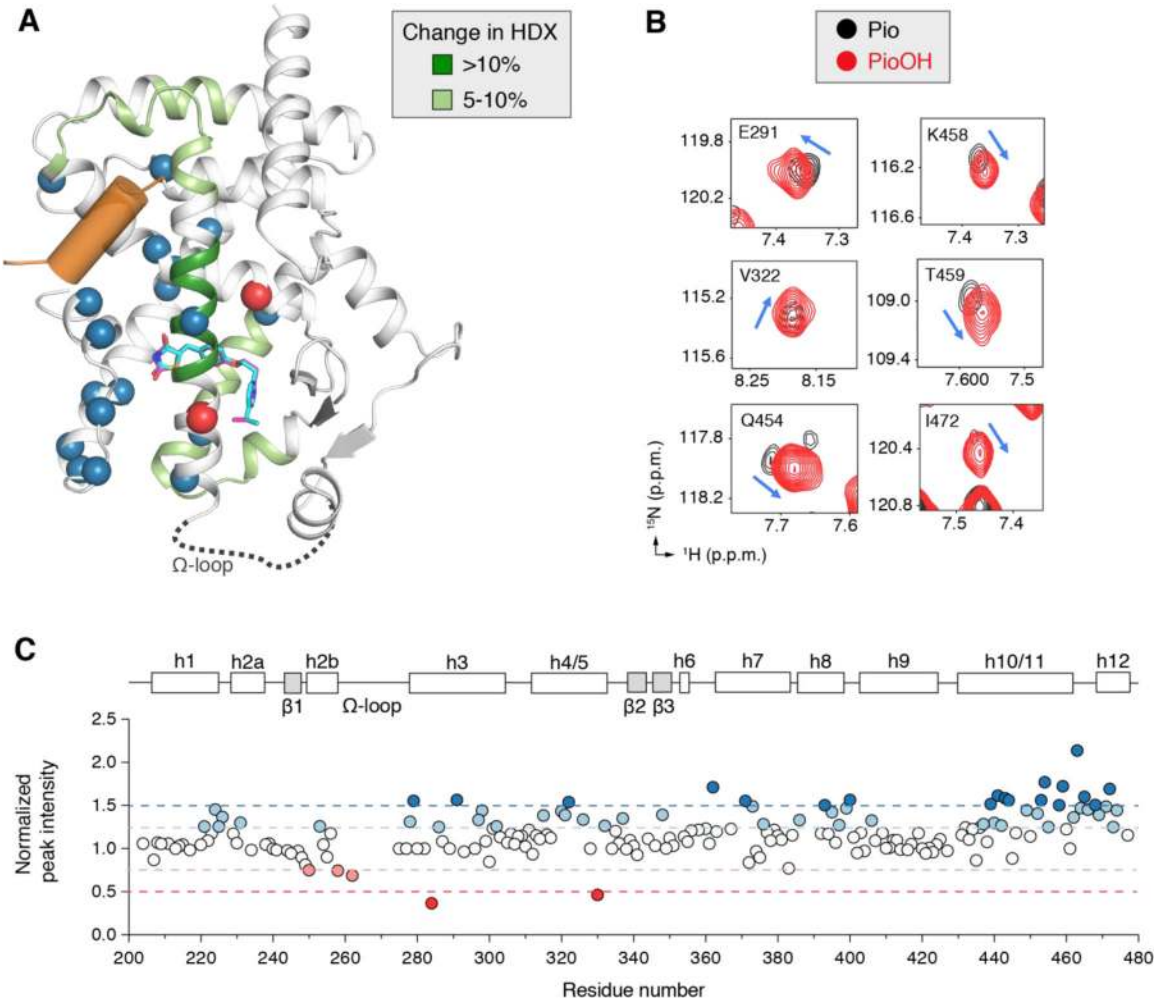

Figure 6.

PioOH enhances stabilization of the AF-2 coregulator interaction surface. (A) Results of HDX-MS and NMR peak intensity analysis displayed on PPARγ LBD crystal structure with a coactivator peptide (orange cylinder) bound to the AF-2 surface (PDB code 2PRG, chain A); Pio and PioOH ligand binding modes are displayed as blue and magenta sticks, respectively. Regions of the PPARγ LBD that exhibit increased protection from HDX bound to PioOH relative to Pio are colored light or dark green on the cartoon diagram. Residues with increased (blue spheres) or decreased (red spheres) NMR peak intensity when PPARγ LBD is bound to PioOH, relative to PPARγ LBD bound to Pio, in the differential NMR analysis are also displayed. (B) Representative residues with increased NMR peak intensity in the PioOH-bound form relative to the Pio-bound form. (C) Differential NMR peak intensity analysis plotted by residue. PioOH-bound peak intensities are normalized to Pio-bound peak intensities; residues are highlighted with normalized peak intensities greater than (blue) or less than (red) 1.25x and 1.5x the average normalized peak intensity difference. PPARγ LBD structural elements are depicted linearly above the graph.

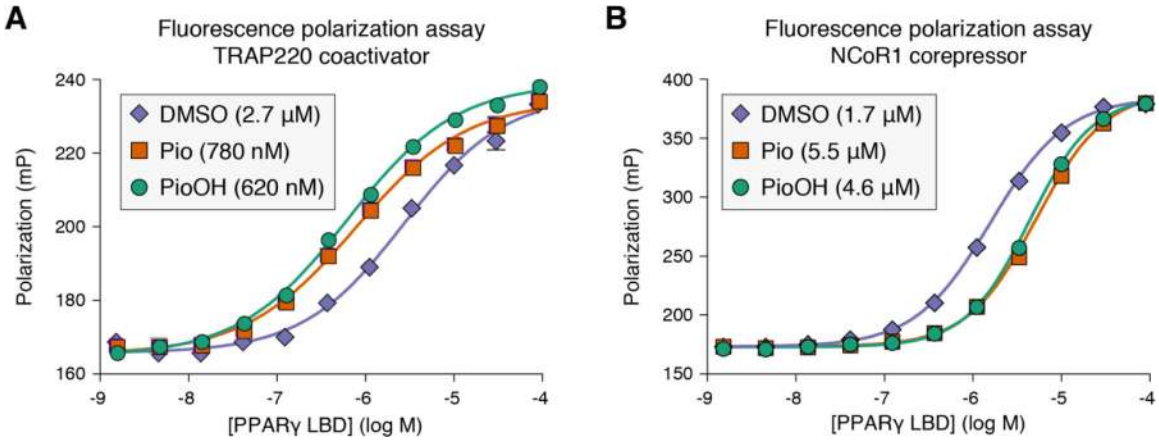

Figure 7.

Pio hydroxylation affects coactivator and corepressor binding to PPARγ LBD. (A,B) Fluorescence polarization assays determined the binding affinities of FITC-labeled peptides derived from the (A) TRAP220 coactivator and (B) NCoR corepressor. Average peptide affinity values from individual experiments for TRAP220 were 2.8 ± 0.035 μM (DMSO), 780 ± 14 nM (Pio), and 600 ± 28 nM (PioOH) ($P<0.05$ comparing Pio and PioOH). Average peptide affinity values from individual experiments for NCoR1 were 2.2 ± 0.49 μM (DMSO), 6.6 ± 1.1 μM (Pio), and 5.5 ± 0.89 μM (PioOH) ($P\sim0.5$ comparing Pio and PioOH).

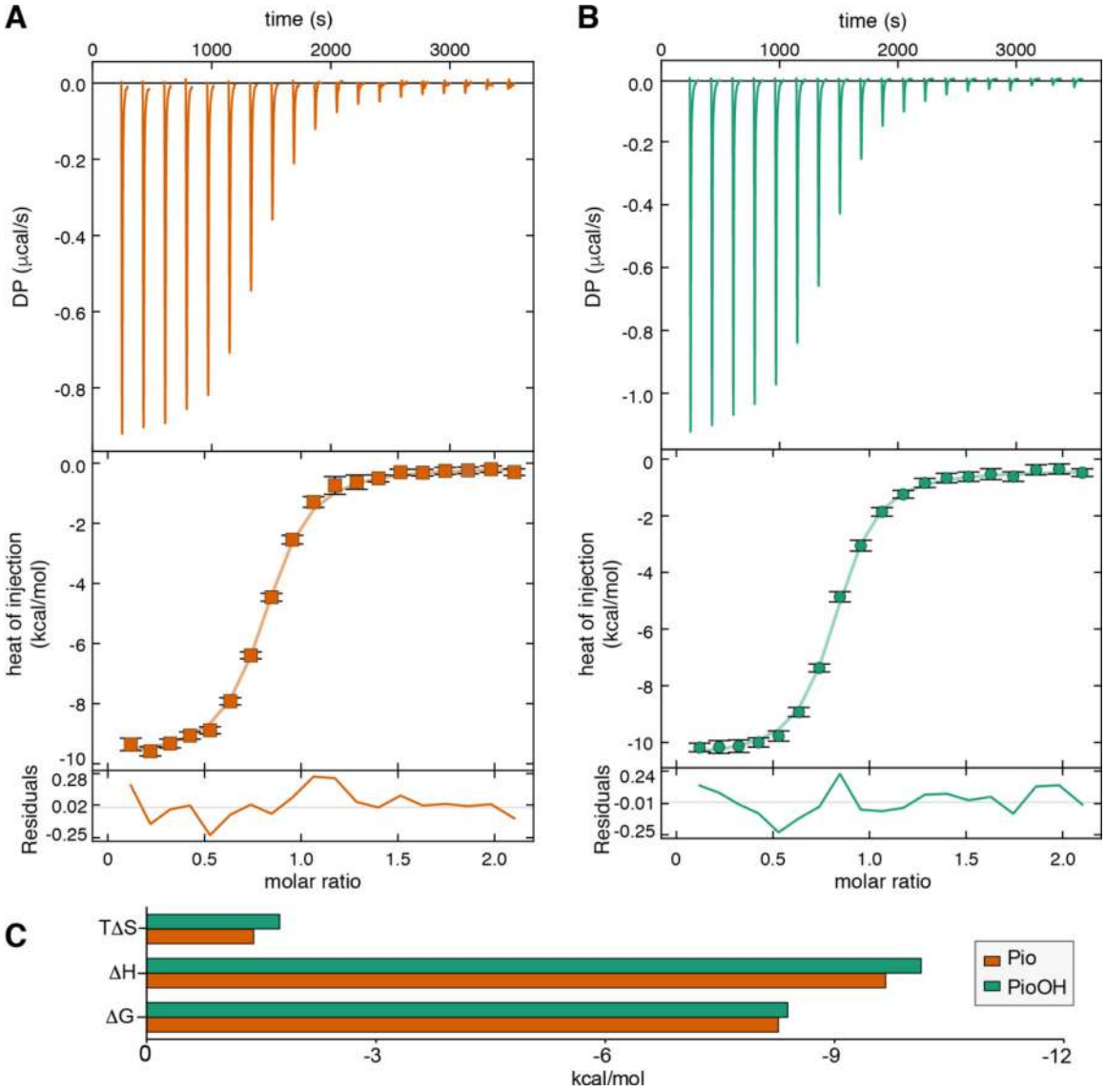

Figure 8.

PioOH stabilizes coactivator binding to the PPARγ LBD. (A,B) Representative thermograms and normalized plotted data from ITC analysis of TRAP220 binding to Pio- (A) or PioOH- (B) bound PPARγ LBD. (C) Thermodynamic parameters from an unbiased global analysis of two replicate runs per condition.

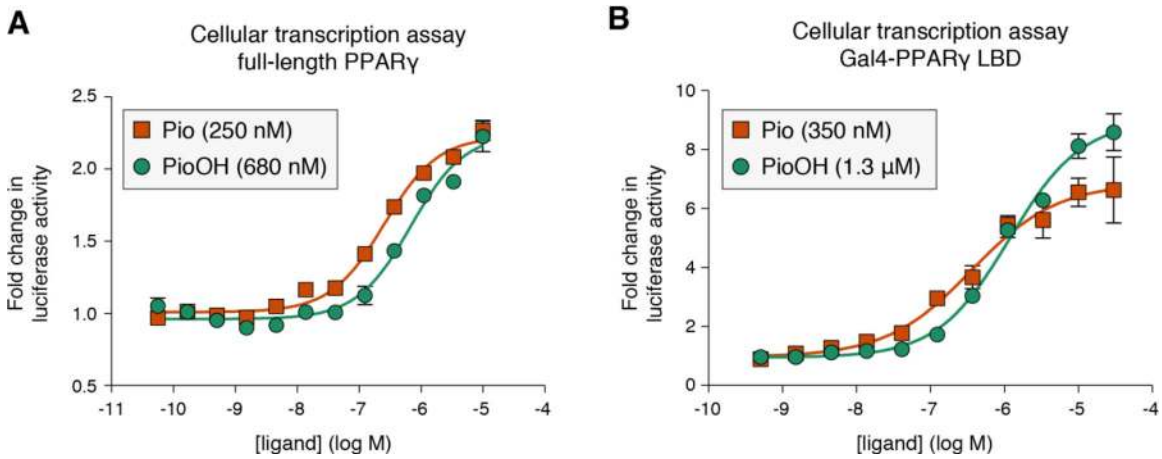

Figure 9.

PioOH induces a modestly greater transcriptional efficacy of the PPARγ LBD. (A) Full-length PPARγ luciferase transcriptional assay using a 3xPPRE-luciferase reporter plasmid in HEK293T cells treated with increasing concentrations of Pio or PioOH; data are normalized to DMSO control treated cells. Legend shows ligand-dependent luciferase activity EC_{50} values; average EC_{50} from independent experiments are 230 ± 0.032 nM (Pio) and 620 ± 120 nM (PioOH) ($P<0.05$) (B) PPARγ LBD-Gal4 DBD luciferase transcriptional assay using a 5xUAS-luciferase reporter plasmid in HEK293T cells treated with increasing concentrations of Pio or PioOH; data are normalized to DMSO control treated cells. Average EC_{50} from independent experiments are 300 ± 0.045 nM (Pio) and 1.3 ± 0.0065 μM (PioOH) ($P<0.01$).

Table 1.

Crystallography data collection and refinement statistics.

	PPARγ LBD bound to 1-hydroxypioglitazone (PioOH)
Data collection	BCSB-5.0.2
Space group	C 1 2 1
Cell dimensions	
a, *b*, *c* (Å)	93.08, 61.85, 119.67
α, *β*, *γ* (°)	90, 102.73, 90
Resolution	49.12–1.88 (1.95–1.88)
R_{pim}	0.056 (0.456)
I / σ(I)	4.93 (1.29)
*CC*1/2 in highest shell	0.618
Completeness (%)	97.33 (95.12)
Redundancy	1.8
Refinement	
Resolution (Å)	1.88
No. of reflections	98149
R_{work}/R_{free} (%)	22.05/25.53
No. of atoms	
Protein	4147
Water	250
B-factors	
Protein	46.19
Ligand	52.84
Water	45.78
Root mean square deviations	
Bond lengths (Å)	0.008
Bond angles (°)	0.95
Ramachandran favored (%)	96.08
Ramachandran outliers (%)	1.37
PDB accession code	6DHA

Values in parentheses indicate highest resolution shell.

Table 2.

Affinity results from AutoDock Vina for the most favorable pose of each metabolite stereoisomer or enantiomer. None of the crystallographic water molecules interacting with PioOH in the PioOH-bound PPARγ LBD crystal structure were included during the docking. The data indicate log scale values of the predicted binding affinities. The poses for which the most favorable pose is not similar to the crystal pose of PioOH are denoted N/A.

	(S)	**(R)**	**(S, S)**	**(R, R)**	**(S, R)**	**(R, S)**
Pioglitazone	−8.9	N/A				
M-I	−6.8	−6.2				
M-II [1]			N/A	−8.5	−8.9	N/A
M-III	N/A	N/A				
M-IV (PioOH) [2]			N/A	N/A	N/A	N/A
M-V	N/A	N/A				
M-VI	N/A	N/A				

Table 3.

Affinity results from AutoDock Vina for the most favorable pose of each metabolite stereoisomer/enantiomer. HOH709 crystallographic water molecule was included during the docking procedure. The data indicate log scale values of the predicted binding affinities. The poses for which the most favorable pose is not similar to the crystal pose of PioOH are denoted N/A.

	(S)	**(R)**	**(S, S)**	**(R, R)**	**(S, R)**	**(R, S)**
Pioglitazone	−9.1	−8.5				
M-I	−6.8	−6.2				
M-II [1]			−8.9	−8.6	−9.1	N/A[3]
M-III	−9.0	N/A[3]				
M-IV (PioOH) [2]			−8.9	−8.4	−9.1	−8.4
M-V	−9.1	−8.6				
M-VI	−9.1	−8.7				

Table 4.

Affinity results from AutoDock Vina for the most favorable pose of each metabolite stereoisomer/enantiomer. The average position of the HOH628 and HOH692 crystallographic water molecules were included during the docking. The data indicate log scale values of the predicted binding affinities. The poses for which the most favorable pose is not similar to the crystal pose of PioOH are denoted N/A.

	(S)	**(R)**	**(S, S)**	**(R, R)**	**(S, R)**	**(R, S)**
Pioglitazone	−9.0	−8.0				
M-I	−6.8	−6.2				
M-II [1]			−9.0	−8.7	−9.2	−8.3
M-III	−9.1	−8.5				
M-IV (PioOH) [2]			N/A[3]	−8.4	−8.9	−8.5
M-V	−8.9	−8.6				
M-VI	−9.0	−8.5				

Table 5.

Affinity results from AutoDock Vina for the most favorable pose of each enantiomer metabolites. The bridging water molecules were included during the docking. The data indicate log scale values of the predicted binding affinities.

	(S)	(R)	(S, S)	(R, R)	(S, R)	(R, S)
Pioglitazone	−9.1	−8.5				
M-I	−6.8	−6.2				
M-II [1]			−9.1	−8.8	−9.2	−8.5
M-III	−9.1	−8.5				
M-IV (PioOH) [2]			−9.0	−8.7	−9.1	−8.5
M-V	−9.2	−8.7				
M-VI	−9.2	−8.7				

Table 6.

Unbiased global fitted ITC parameters for TRAP220 peptide titrated into PPARγ LBD.

Ligand	Stoichiometry	K_d (nM)	ΔG (kcal/mol)	ΔH (kcal/mol)	ΔS (kcal/mol*K)
Pio	0.783	871 (68.3% CI: 740 to 1020)	−8.39	−10.136 (68.3% CI: −10.3589 to −9.9186)	−5.856
PioOH	0.792	708 (68.3% CI: 606 to 823)	−8.27	−9.668 (68.3% CI: −9.8940 to 9.4541)	−4.669

68.3% CI = confidence interval provided by SEDPHAT analysis of two independent ITC runs.